Available online at www.sciencedirect.com

ScienceDirect

Solar Energy 109 (2014) 144–152

SOLAR ENERGY

www.elsevier.com/locate/solener

Electrical characteristics of thin-film CdS/CdMgTe heterostructure for tandem solar cells

L.A. Kosyachenko [a,*], T.I. Mykytyuk [a], I.M. Fodchuk [a], O.L. Maslyanchuk [a], O.S. Martinez [b,c], E.R. Pérez [b], X. Mathew [b]

[a] Chernivtsi National University, Kotsyubinsky Str. 2, 58012 Chernivtsi, Ukraine
[b] Instituto de Energías Renovables, Universidad Nacional Autonoma de Mexico, Temixco, Morelos 62580, México
[c] Centro del Cambio Global y la Sustentabilidad en el Sureste, Villahermosa, Tabasco 86080, México

Received 17 March 2014; received in revised form 13 August 2014; accepted 14 August 2014
Available online 14 September 2014

Communicated by: Associate Editor Takhir Razykov

Abstract

Charge transport mechanism in thin-film CdS/$Cd_{1-x}Mg_xTe$ ($x = 0.08$) heterostructure are investigated. It is shown that the measured *I–V* characteristics and their temperature dependence are described well in terms of the Sah–Noyce–Shockley theory of generation–recombination in the diode space-charge region. A comparison of the experimental data with the theoretical results allowed determining the material and diode parameters such as the resistivity and hole density in the valence band of the film, the energy of the Fermi level and the barrier height at the interface, the lifetimes of charge carriers and the ionization energy of the generation–recombination center. It is also shown that low resistivity of the $Cd_{1-x}Mg_xTe$ absorber layer causes too low barrier height in the heterostructure and unacceptably high electrical losses in the solar cell.

Keywords: CdMgTe solar cells; Charge transport mechanisms; Tandem solar cells

1. Introduction

During the past decades, thin-film technology as an alternative to solar modules based on single- and poly-silicon wafers are being developing rapidly. The most common PV materials that used in the mass production of thin-film modules are amorphous silicon (a-Si), CdTe, and $CuIn_xGa_{1-x}Se_2$ (CIGS). The efficiency of small area laboratory samples of CdS/CdTe solar cells increases year by year and now stands at 20.4% under AM1.5 solar radiation (First Solar, Inc., 2014). However, the efficiency of large area CdTe solar modules had reached only up to 16.1% (First Solar, Inc., 2012). Since this efficiency is about half of the theoretical limit (28–30%), work to improve the CdTe module efficiency is extremely relevant.

One way to improve the efficiency of CdTe modules is the use of tandem devices, where the two cells (sub-cells) with different bandgap semiconductors are superimposed one layer on another. The bandgap of the top sub-cell is larger than that of the bottom one, therefore the part of radiation passed through the top cell is absorbed in the bottom cell depending on the bandgap, and hence the efficiency of such tandem solar cell is higher than a single junction device. Ternary alloy semiconductors of CdTe with Zn, Mn and Mg can achieve the required bandgap criterion for top sub-cells. In order to achieve current matching

* Corresponding author. Tel.: +380 372 244 221; fax: +380 372 551 809.
E-mail address: l.a.kosyachenko@gmail.com (L.A. Kosyachenko).

http://dx.doi.org/10.1016/j.solener.2014.08.029
0038-092X/

which is necessary for two-terminal tandem solar cell and to obtain maximum efficiency the desired bandgap of the top cell absorber layer should be in the range 1.6–1.8 eV (Coutts et al., 2001). The efficiency of a two-terminal tandem polycrystalline thin-film solar-cell is predicted to reach approximately 25% using realistic parameters for materials and assuming that the performances of the individual sub-cells will be close to the corresponding record-efficiency single-junction cells (Coutts et al., 2003).

It is known that the bandgap of the ternary alloy $Cd_{1-x}Mg_xTe$ can be easily tuned from ~1.5 to 3.5 eV (x = 0–1), and hence this material is a promising candidate for developing the top sub-cell in tandem devices. The close match of the lattice constant of MgTe with CdTe (the mismatch is as low as 0.7% (Waag et al., 1993) and the apparent complete miscibility of MgTe in CdTe and the rapid increase in the bandgap with Mg content gives the flexibility to prepare top-cell material with the appropriate bandgap for current matching. For the above top-cell, a suitable absorber material for the bottom sub-cell can be the well-studied CIGS and $Hg_xCd_{1-x}Te$ alloys with a bandgap in the range of 1–1.1 eV.

In order to develop $Cd_{1-x}Mg_xTe$ as a potential top-cell absorber material in thin-film tandem solar cell, the structure, morphology, electrical, optical and optoelectronic properties of this material have been studied quite extensively (Mathew et al., 2009; Martinez et al., 2009; Tatarenko et al., 1997; Ihn et al., 2004; Dhere et al., 2007). In the literature, the obtained results are discussed giving emphasis for their impact on device parameters such as: the short-circuit current, the open circuit voltage, the fill factor and, ultimately, the photoelectric conversion efficiency. Unfortunately, information about another key characteristic which determines the basic photoelectric parameters of a solar cell, i.e., the current–voltage (I–V) characteristic of $CdS/Cd_{1-x}Mg_xTe$ heterostructure, is practically absent in the literature with very few exceptions.

The results discussed in this paper will fill the above mentioned gap to some extent. We demonstrate for the first time that the I–V characteristics of thin-film $CdS/Cd_{1-x}Mg_xTe$ solar cell can be described in detail by the theory based on the model developed for the linearly graded Si p–n junction by Sah et al. (1957) and modified and adapted to thin-film CdS/CdTe heterostructure in Refs. Kosyachenko (2006) and Kosyachenko and Toyama (2014). A comparison of the modeling results with the experimental data allows us to determine the main parameters of the material used and the diode structure such as: resistivity of the $Cd_{1-x}Mg_xTe$ absorber, concentration of holes in the valence band, energy of the Fermi level, the width and the barrier height at the surface, the lifetimes of charge carriers, and the ionization energy of the generation–recombination center. The obtained results allow us to formulate some recommendations to improve the performance of the $CdS/Cd_{1-x}Mg_xTe$ solar cell.

2. Samples

CdS and $Cd_{1-x}Mg_xTe$ films were deposited on glass substrates coated with SnO_2:F (Tec7) obtained from Pilkington Group Limited. In order to meet the top-cell bandgap criteria as mentioned previously and to minimize the perturbations due to the incorporation of Mg in the lattice of CdTe, we selected the bandgap in the lower limit by fixing the deposition parameters such that $x = 0.08$. The $Cd_{0.92}Mg_{0.08}Te$ films with the bandgap close to 1.6 eV and thicknesses of 1.3 μm were prepared by vacuum co-evaporation of CdTe and Mg on CdS/Tec7 substrates heated to 300–400 °C. The CdS films of about 0.1 μm thickness were prepared by sputter deposition at 250 °C. The metal back contacts to the devices were 3 nm Cu/30 nm Au. Similar to CdTe based solar cells, $CdS/Cd_{1-x}Mg_xTe$ devices showed dependence on the vapor chloride annealing temperature and Cu diffusion process (Mathew et al., 2009; Martinez et al., 2009). The vapor chloride annealing was done in a furnace at 387 °C for 5–10 min under a continuous dry air flow.

The bandgap E_g of the grown $Cd_{1-x}Mg_xTe$ layers was determined by measuring their optical transmission assuming that the absorption coefficient α in the vicinity of the absorption edge is proportional to $(h\nu - E_g)^{1/2}/h\nu$, which is true for direct-gap semiconductor, and applicable for $Cd_{1-x}Mg_xTe$ up to $x \approx 0.7$ (Dhere et al., 2006). The dependence of α on $h\nu$, obtained from the measured optical transmittance of $Cd_{0.92}Mg_{0.08}Te$ layer with the theory for direct-gap semiconductor is shown in Fig. 1. As seen, good agreement between theory and experiment is observed which allows a sufficiently accurate determination of the semiconductor bandgap.

The data in the literature on the relationship of the bandgap to the Mg content in $Cd_{1-x}Mg_xTe$ are quite contradictory (Dhere et al., 2006; Waag et al., 1993; Hartman

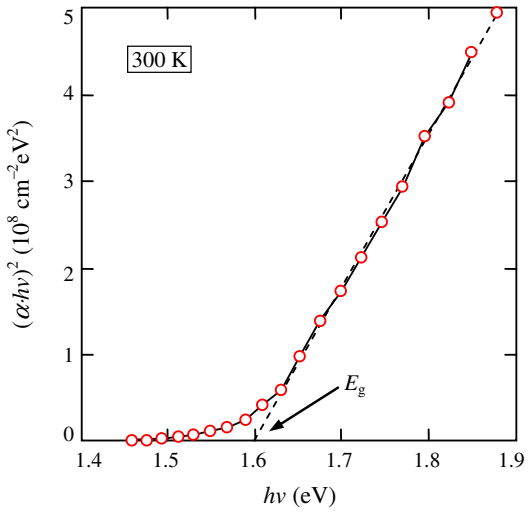

Fig. 1. Correlation of the experimental curve $\alpha(h\nu)$ with the dependence $\alpha \propto (h\nu - E_g)^{1/2}/h\nu$ for the $Cd_{0.92}Mg_{0.08}Te$ layer at room temperature.

et al., 1996). One can assume that this is due to the peculiarities of deposition technique and subsequent heat treatment of polycrystalline $Cd_{1-x}Mg_xTe$ layers. As in the case of CdTe, during the widely used $CdCl_2$ treatment, significant recrystallization leading to grain growth and grain coalescence apparently occur in the $Cd_{1-x}Mg_xTe$ film. No less important is also the fact that a morphology in the form of ordered columns perpendicular to the substrate is observed in the $Cd_{1-x}Mg_xTe$ layer similar to that in the CdTe layer (see Bonnet, 2003; McCandless and Sites, 2011 and references therein).

In order to determine the Mg content in the films, we used the results of thorough studies presented in Ref. Compaan et al. (2008). It has been shown that the bandgap narrows considerably upon $CdCl_2$ treatment (from 1.529 to 1.476 eV measured at room temperature) mainly due to change in film stoichiometry associated with the affinity of Mg towards oxygen, relaxation of strain, increase in grain size, reducing the width of grain boundaries, the oxidized compounds at the surface of films, improving the homogenous and repeatable cells (Compaan et al., 2008; Rejon et al., 2013; Hernández-Rodríguez et al., 2014; Toma et al., 2014). It was shown in Compaan et al. (2008) that when $x = 0.15$ and 0.3, the value of E_g upon $CdCl_2$ treatment amounts to 1.71 and 1.98 eV, respectively. It follows that at higher values of x, the deviation from linearity occurs. It is easy to verify that for the linear approximation the value $E_g = 1.71$ eV at $x = 0.15$ gives the formula:

$$E_g(x) = 1.476 + 1.56x. \quad (1)$$

From Eq. (1), $x = 0.08$ is obtained for the $Cd_{1-x}Mg_xTe$ absorber layer with the bandgap 1.6 eV.

3. Theoretical model for interpretation of experimental results

Fig. 2a shows a typical example for measured I–V characteristics of thin-film $CdS/Cd_{0.92}Mg_{0.08}Te$ heterostructure. As seen, the forward current at $V > 0.5$ V exceeds the reverse current by more than 4–5 orders of magnitude, i.e., the heterostructure has pronounced rectifying properties. Exponential increase of forward current with voltage $I \propto \exp(qV/nkT)$ for the ideality factor $n \approx 2$ in the range $V = 0.05$–0.45 V is the most characteristic for this and other studied samples (q is the electron charge, k is the Boltzmann constant). At $V > 0.45$ V, the I–V characteristic deviates from this exponential relationship, which is usually, explained by the voltage drop across the series resistance R_s of the neutral part of the absorber layer.

The value of the series resistance R_s can be found from the dependence of the *differential* resistance $R_{dif} = dV/dI$ of the diode structure under forward bias as shown in Fig. 2b for the investigated sample. As can be seen, at $V > 0.7$ V, there is a horizontal part on the dependence $R_{dif}(V)$ at the level of $6.3 \times 10^3\ \Omega$. At such a high forward voltage, the space-charge region evidently disappears, and the voltage drop across the resistance of the material dominates. Under such conditions, the dependence of current on voltage is linear; the value of R_{dif} is constant and equal to the series resistance R_s of the $Cd_{0.92}Mg_{0.08}Te$ layer.

When the series resistance is taken into account, the I–V curve modifies at $V > 0.45$ V as shown by triangle markers in Fig. 2a. As a result, the exponential dependence of the current on the voltage extends approximately for an order of magnitude, nevertheless at $V > 0.55$ V deviation from the exponential dependence occurs. The latter is explained within the theory of recombination by the gradual narrowing of the space-charge region (SCR) when V approaches to the diffusion potential $V_{bi} = \varphi_{bi}/q$. The value φ_{bi} is the barrier height from the semiconductor side (equal to the value of the band bending in the CdTe layer near the interface), which is one of the most important parameters of heterostructure based on CdTe and $Cd_{1-x}Mg_xTe$. The higher the barrier φ_{bi}, the greater the depletion layer width and the electric field that separates photogenerated electrons and holes preventing their recombination. Note also that the *reverse* current at V above a few kT/q increases with applied voltage, rather than is constant, as in the case of thermionic emission mechanism.

The assumption of the generation–recombination mechanism of charge transport is quite acceptable because the $Cd_{1-x}Mg_xTe$ layer apparently contains many impurities and defects with the possibility of their levels located near the middle of the gap. According to the Shockley–Read–Hall statistics, such impurities or defects are effective recombination and generation centers under forward and reverse bias, respectively. As shown below, the model of generation–recombination in the SCR can explain well the observed I–V characteristics of $CdS/Cd_{1-x}Mg_xTe$ heterostructure just as it is done for the CdS/CdTe solar cells (Kosyachenko, 2006; Kosyachenko and Toyama, 2014).

According to the Sah–Noyce–Shockley theory, the generation–recombination rate in the cross section x of the SCR at the voltage V is determined by the expression (Sah et al., 1957):

$$U(x,V) = \frac{n(x,V)p(x,V) - n_i^2}{\tau_{po}[n(x,V) + n_1] + \tau_{no}[p(x,V) + p_1]}, \quad (2)$$

where $n(x, V)$ and $p(x, V)$ are the carrier concentrations in the conduction and valence bands within the SCR, respectively; n_i is the intrinsic carrier concentration in the semiconductor; $\tau_{no} = 1/\sigma_n \upsilon_{th} N_t$ and $\tau_{po} = 1/\sigma_p \upsilon_{th} N_t$ are the lifetimes of electrons and holes in highly p-type and highly n-type semiconductor; σ_n and σ_p are the capture cross sections of electrons and holes, respectively; υ_{th} is the charge-carrier thermal velocity; N_t is the concentration of the generation–recombination centers.

The quantities n_1 and p_1 in Eq. (2) are determined by the ionization energy of the generation–recombination center E_t measured from the top of the valence band:

$$n_1 = N_c \exp\left[-\frac{E_g - E_t}{kT}\right], \quad (3)$$

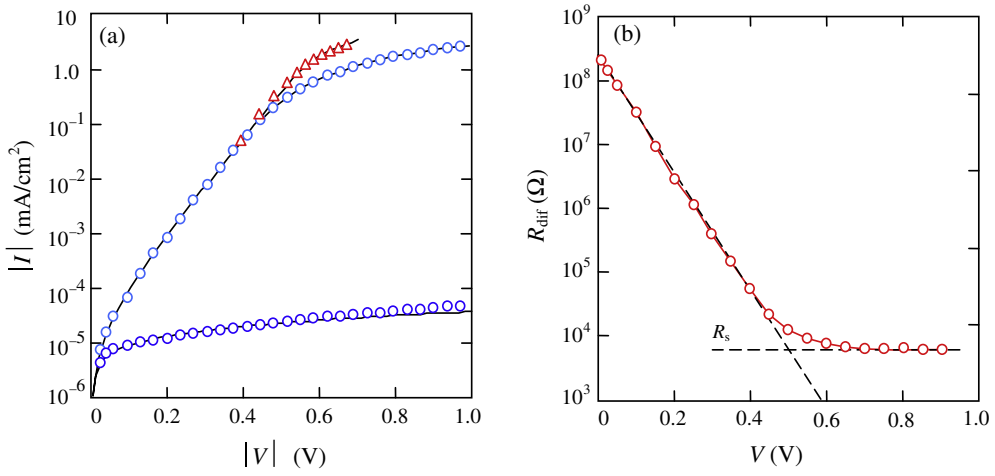

Fig. 2. (a) Room temperature I–V characteristic of CdS/$Cd_{0.92}Mg_{0.08}Te$ solar cell. The measured curve and the curve obtained by taking into account the voltage drop across the series resistance are shown by circles and triangles, respectively. The solid lines correspond to the calculated curves. (b) Dependence of the differential resistance of the sample under forward bias showing the presence of the series resistance R_s in the diode circuit.

$$p_1 = N_v \exp\left[-\frac{E_t}{kT}\right] \tag{4}$$

where $N_c = 2(m_n \kappa T/2\pi\hbar^2)^{3/2}$ and $N_v = 2(m_p \kappa T/2\pi\hbar^2)^{3/2}$ are the effective densities of states in the conduction and valence bands, and m_n and m_p are the effective electron and hole masses, respectively.

The expressions for $n(x, V)$ and $p(x, V)$ in the SCR take the form (Kosyachenko, 2006; Kosyachenko and Toyama, 2014):

$$n(x,V) = N_v \exp\left[-\frac{E_g - \Delta\mu - \varphi(x,V) - qV}{kT}\right], \tag{5}$$

$$p(x,V) = N_v \exp\left[-\frac{\Delta\mu + \varphi(x,V)}{kT}\right], \tag{6}$$

where $\Delta\mu$ denotes the energy difference between the Fermi level and the valence band top in the bulk part of the $Cd_{1-x}Mg_xTe$ layer.

In Eqs. (5) and (6), $\varphi(x, V)$ is the potential energy of the charge carriers in the SCR of the $Cd_{1-x}Mg_xTe$ layer. This potential energy term can be described similar to the case of an abrupt asymmetric p–n heterojunction by the parabolic law (Sze and Ng, 2006):

$$\varphi(x,V) = (\varphi_{bi} - qV)\left(1 - \frac{x}{W}\right)^2, \tag{7}$$

where W is the width of the SCR:

$$W = \sqrt{\frac{2\varepsilon\varepsilon_o(\varphi_{bi} - qV)}{q^2(N_a - N_d)}}. \tag{8}$$

Here, ε is the relative permittivity of the semiconductor, ε_o is the permittivity of vacuum, and $N_a - N_d$ is the concentration of uncompensated acceptors in the $Cd_{1-x}Mg_xTe$ layer. The potential energy $\varphi(x)$ in Eq. (7) is measured downward from the top of the valence band in the neutral part of the $Cd_{1-x}Mg_xTe$ (in Eq. (8), we neglect kT in comparison with φ_{bi}).

The recombination current density under forward bias and the generation current under reverse bias are found by the integration of $U(x, V)$ throughout the entire depletion layer:

$$J = \int_0^W U(x,V)dx. \tag{9}$$

4. Comparison of the calculated and measured results

Fig. 2a compares the measured I–V characteristic of the CdS/$Cd_{0.92}Mg_{0.08}Te$ solar cell (circles) with the calculation results (solid lines). In the calculation, it was necessary to know the energy of the Fermi level $\Delta\mu$ (appearing in Eqs. (5) and (6)) with respect to valance band in the bulk part of the $Cd_{1-x}Mg_xTe$ layer. The $\Delta\mu$ value can be found from the resistivity ρ using the resistance of the $Cd_{1-x}Mg_xTe$ layer $R_s = 6.3 \times 10^3\ \Omega$, the diode area 0.031 cm^2 and thickness of the layer 1.3 μm. Knowing $\rho = 1.3 \times 10^6\ \Omega$ cm, one can find the hole concentration in the valence band $p = 1/q\rho\mu_p = 1.2 \times 10^{11}\ cm^{-3}$ (for $\mu_p = 40\ cm^2/(V\ s)$ (Gloeckler et al., 2003) and next the Fermi level energy $\Delta\mu = kT\ln(N_v/p) = 0.45$ eV.

Other parameters of the $Cd_{1-x}Mg_xTe$ layer are the concentration of uncompensated impurities $N_a - N_d$ (which determines the width of the SCR) and the lifetime of charge carriers τ_{no} and τ_{po} in the SCR. According to the Sah–Noyce–Shockley theory, the forward current within the portion of I–V relationship, where $I \propto \exp(qV/2kT)$, is determined by the $[\tau_{no}\tau_{po}(N_a - N_d)]^{1/2}$ value (Kosyachenko, 2006). To prevent recombination losses in the SCR, its width should be equal or less than ~0.3 μm, which according to Eq. (8) corresponds to the concentration of uncompensated acceptor $(N_a - N_d) \approx 10^{16}\ cm^{-3}$ (Kosyachenko et al., 2013). Taking $N_a - N_d = 10^{16}\ cm^{-3}$, in order for the calculated current values to match with the experimental results in Fig. 2a, one should assume that $(\tau_{no}\tau_{po})^{1/2}$ should be

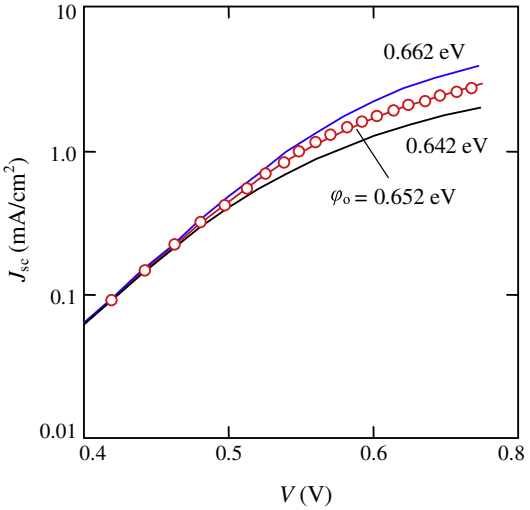

Fig. 3. Comparison of the calculation results with the experimental data under forward bias voltages close to the built-in potential $V_{bi} = \varphi_{bi}/q$.

equal to 0.6 ns, which is close to the carrier lifetime in CdTe thin films (Sites and Pan, 2007; Gessert et al., 2009). Note that in thin-film CdTe, the carrier lifetime is in the range from 10^{-10} to 2×10^{-9} s. For such lifetime range, in order for the calculated values of current match the experimental data, $N_a - N_d$ must be between 10^{15} and 10^{17} cm^{-3}.

It should be emphasized that even taking into account the voltage drop across the series resistance R_s, there is a deviation of the experimental from the relationship $I \propto \exp(qV/2kT)$ at $V > 0.5$ V as shown in Fig. 2a. As previously mentioned, when the applied voltage approaches to the built-in potential $V_{bi} = \varphi_{bi}/q$, the width of the SCR becomes quite small and, therefore, the dependence of the recombination current on voltage reduces. Obviously, the voltage at which the dependence reduces is associated with the barrier height φ_{bi}. This is confirmed by comparing the experimental data with the calculation results for different φ_{bi} at $V > 0.4$ V (300 K), which is shown in Fig. 3. As seen, the best fit to the experimental data takes place for $\varphi_{bi} = 0.652$ eV, whereas a small deviation of ± 0.01 eV leads to a substantial discrepancy between the calculated and the experimental data. Thus, such a comparison of the calculated and experimental data can be regarded as a method for determining the barrier height φ_{bi} with a good accuracy.

From Fig. 2a it is clear that the calculation results agree very well with the measured forward current in the range $V < 0.5$ V, where the current follows the dependence $I \propto [\exp(qV/nkT) - 1]$ with the ideality factor $n = 1.9$ (rather than 2) within more than 4 orders of magnitude. The deviation of n from 2 is explained by the fact that according to the theory, the dependence of the recombination current on the voltage is determined not only by the exponent $\exp(qV/2kT)$, but also by the pre-exponential factor $(E_g - 2\Delta\mu - qV)^{-1/2}$, which somewhat promotes an increase in current with V and thus reduces the ideality factor (Kosyachenko and Toyama, 2014; Kosyachenko et al., 2013). The theory also gives a precise description of the $J(V)$ dependence in the range $V = 0.5$–0.7 eV in Fig. 2a (taking into account the voltage drop across the series resistance), if to take $\varphi_{bi} = 0.652$ eV.

One might think that the above coincidence between the theory and experiment is achieved by varying too many parameters. But it should be kept in mind that these parameters affect the J–V characteristic *differently*. In fact, (i) the value of the forward current over an exponential portion of the J–V dependence is determined exclusively by the product of the "effective" carrier lifetimes in the SCR $(\tau_{no}\tau_{po})^{1/2}$ and the concentration of uncompensated acceptors $N_a - N_d$ in the CdTe absorber; (ii) the ionization energy of the generation–recombination center E_t determines practically only the reverse current with high accuracy. A small shift of the generation–recombination level from the mid-gap causes a significant decrease of the reverse current, whereas the forward current at $V > 0.1$ V is unchanged; (iii) the barrier height φ_{bi} affects the J–V relationship only at high forward bias, where the current deviates from the exponential dependence; (iv) the energy of the Fermi level $\Delta\mu$ is determined from the voltage dependence of the differential diode resistance under forward biases. Thus, an agreement of the calculation results with the experimental data is achieved for a well-defined combination of $\Delta\mu$, φ_{bi}, E_t and the $(\tau_{no}\tau_{po})^{1/2}(N_a - N_d)$ product.

Note that too high value of the Fermi level energy $\Delta\mu = 0.45$ eV (extracted from the voltage dependence of the diode differential resistance) affect adversely the performance of the investigated CdS/CdMgTe solar cell. In fact, the barrier height φ_{bi} decreases when the Fermi level moves away from the valence band ($\varphi_{bi} \approx E_g - \Delta\mu$), which occurs in high resistive materials. But if, on the contrary, the $\Delta\mu$ is made less than 0.1 eV by introducing shallow acceptors in $Cd_{1-x}Mg_xTe$, the barrier height increases to ~1 eV instead of 0.652 eV. As a result, the forward current will deviate from the exponential dependence $J_{sc} \propto \exp(qV/nkT)$ at higher voltage, thus facilitating the achievement of the desired high short-circuit current density J_{sc}. Furthermore, when the resistivity of the absorber layer increases, the *electrical losses* in the solar cell also increases. For example, if $\rho = 10^6\ \Omega$ cm, the voltage drop across the series resistance R_s at $J_{sc} = 20$ mA/cm^2 is equal to 2 V (!).

Summarizing the discussion of the results presented in Fig. 2a, it can be said that the theory is well described not only the forward but also the *reverse* current–voltage characteristic. However, it does not apply to reverse voltages above 0.5 V, when measured values clearly exceed the calculation results. Mechanism of the observed increase in the reverse current will be discussed with the example of another sample with a large deviation of the measured reverse current from the calculated value. The I–V curves of such a sample measured at different temperatures are shown in Fig. 4a. The circles and solid lines show the experimental data and the calculation results, respectively.

For better matching of the calculated and experimental results, the material parameters and diode structure were somewhat changed. When the temperature increases from

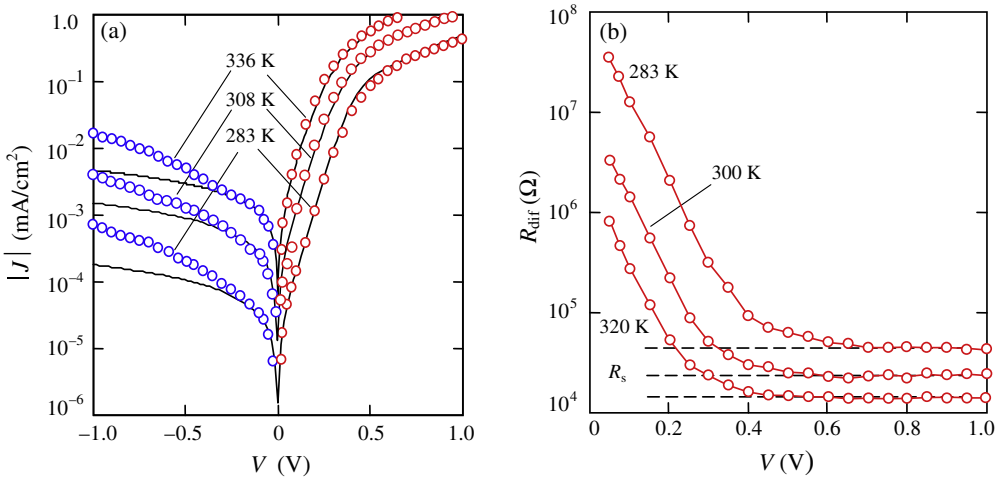

Fig. 4. J–V characteristics (a) and differential resistance under forward bias (b) of $CdS/Cd_{0.92}Mg_{0.08}Te$ cell at different temperatures. The circles and solid lines in this figure (a) show the experimental data and calculated results, respectively.

283 to 336 K, the charge carrier lifetime increases from 0.1 to 1.7 ns due to change in the charge state of the generation–recombination level. At the same time, the barrier height decreases from 0.63 to 0.57 eV with temperature since the energy of the Fermi level increases by approximately the same value. The ionization energy of the generation–recombination center E_t does not change practically with temperature but remained in the range 0.79–0.80 eV.

As seen in Fig. 4a, at different temperatures, the theory describes well the I–V curves under forward bias in a whole range of applied voltages; however, under reverse bias the theory coincides with the experimental data only at voltages less than 0.2–0.3 V. The reverse generation current increases with voltage sub-linearly, but the measured current at higher voltages increases super-linearly. One can assume that the additional increase in the reverse current at voltages higher than 0.2–0.3 V is due to electron tunneling just as it happens in CdS/CdTe solar cells (Kosyachenko and Toyama, 2014).

We are not discussing it in detail since the mechanisms of conduction processes occurring under reverse bias is not so important for the solar cells.

From measurements of the I–V characteristics at different temperatures, additional information about the parameters of the material and the diode structure can be extracted. Fig. 5a shows the temperature dependence of the resistivity of the $Cd_{0.92}Mg_{0.08}Te$ absorber layer, which was obtained from similar plots as shown in Fig. 4b.

As seen, the experimental points in the coordinate $\log\rho$ vs. $1000/T$ gives a good straight line fit, and the slope indicates that the thermal activation energy ΔE of the electrical conductivity of $Cd_{0.92}Mg_{0.08}Te$ is equal to 0.185 eV. Practically the hole in the valance band has the same thermal activation energy, whose concentration increases with temperature from 1.7×10^{10} to 5.4×10^{10} cm^{-3} (Fig. 5b). Also shown in Fig. 5c are the temperature dependences of the reverse current I_{rev} at bias voltage 0.1 V and the so-called saturation current I_o in the diode equation $I = I_o[\exp(qV/1.9kT) - 1]$. From the slope of the best straight line the fit, the thermal activation energy was obtained as $\Delta E = 0.87$ eV. Assume a linear decrease in the bandgap with temperature $E_g(T) = E_g(0) - \gamma T$, where γ is the temperature coefficient of the bandgap, which is equal to 4.52×10^{-4} eV/K for CdTe (Kosyachenko et al., 2011). Then, to obtain $E_g = 1.6$ eV at 300 K for $Cd_{1-x}Mg_xTe$, the $E_g(0)$ value must be set equal to 1.74 eV, i.e. double of the value of $\Delta E = 0.87$ eV. As it is known, if the generation–recombination level is located at the middle of the bandgap (in our case $E_t = 0.79$–0.8 eV), the saturation current I_o and the reverse current at $qV \gg kT$ are proportional to the intrinsic carrier concentration n_i. On the other hand, the thermal ionization energy associated with the intrinsic conductivity of the semiconductor is equal to half of the bandgap at $T = 0$, i.e., $E_g(0)/2 = 0.87$ eV, which coincides with the obtained ΔE value. Thus, the dependences of the forward and reverse currents on the temperature confirm once again the applicability of the generation–recombination theory to the investigated $CdS/Cd_{1-x}Mg_xTe$ solar cells.

It should also be noted that some of the investigated $CdS/Cd_{1-x}Mg_xTe$ solar cells turned out to be shunted. Fig. 6a shows the results of the I–V characteristic measurement of such a sample (shown by circles) and their analysis at 300 K. As seen, on the forward I–V curve at voltages $V < 0.2$ V, the measured currents are significantly higher than the exponential $J_{sc} \propto [\exp(qV/1.9kT) - 1]$ dependence, which is clearly visible at $V < 0.3$ V. In addition, at $V < 0.2$ V the forward and reverse currents are the same in magnitude. These features are a sign of the presence of a shunt in the sample. This is supported by the dependence of the differential resistance on the forward voltage $R_{dif}(V)$ shown in Fig. 6b. When $V > 0.8$ V, the presence of series resistance R_s in the circuit clearly reveals itself. In addition, when $V < 0.1$ V the horizontal portion of the curve is also observed indicating the presence of a shunt, the value of which is equal to 1.07×10^7 Ω.

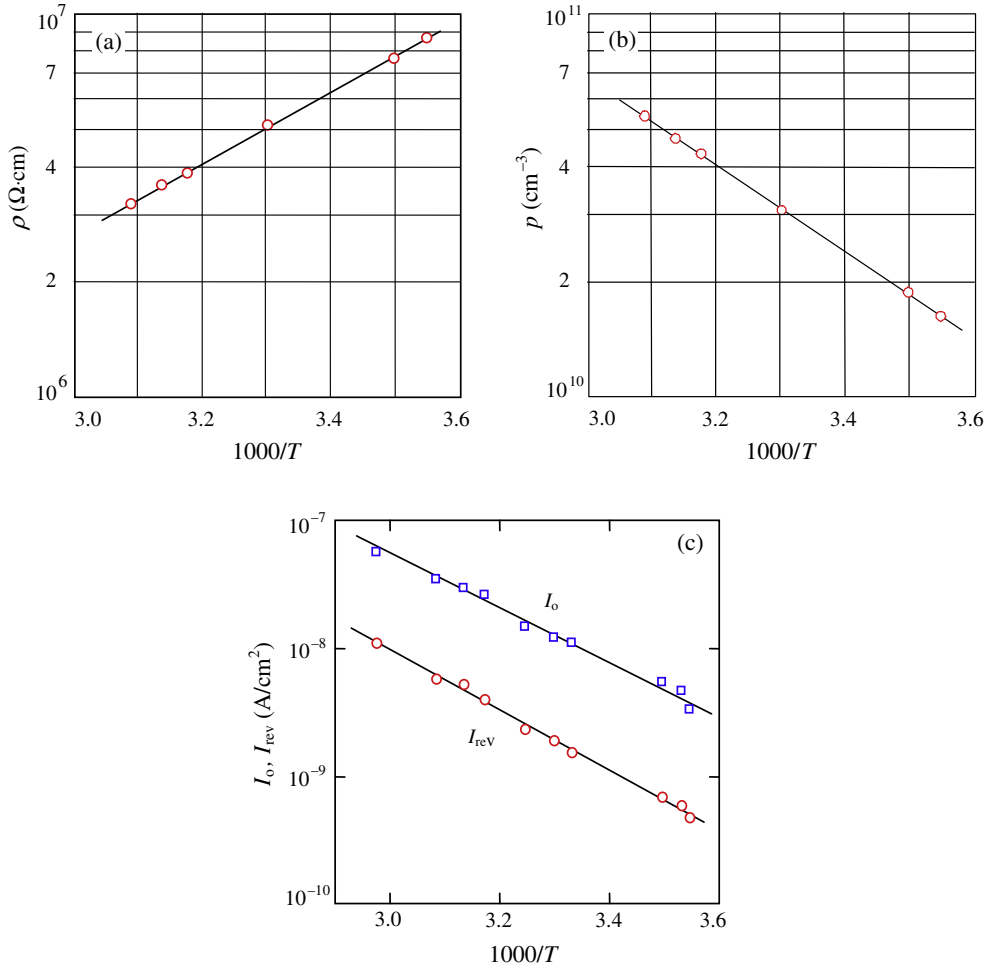

Fig. 5. Temperature dependences of the resistivity (a) and the free hole density (b) in the $Cd_{0.92}Mg_{0.08}Te$ layer, as well as the forward I_o and reverse currents I_{rev} (c).

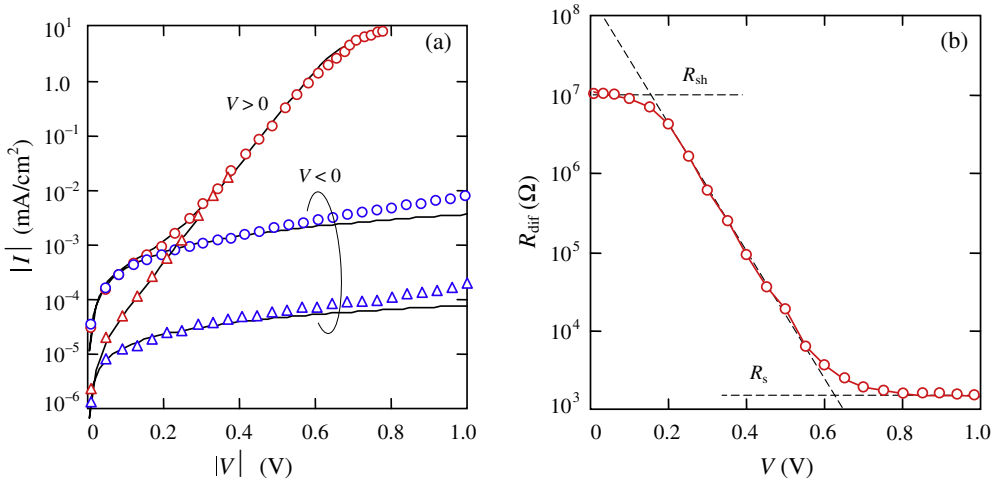

Fig. 6. (a) Room temperature *I–V* characteristic of a CdS/ $Cd_{0.92}Mg_{0.08}Te$ cell with shunting. The circles and triangles show respectively the measured curve and that obtained by subtracting the shunt current from measured current. The solid lines show the corresponding calculated curves. (b) Dependence of the differential resistance of the sample under forward bias showing the presence of shunt R_{sh} and series resistance R_s.

Obviously, taking into account shunting, the measured current can be written as the sum of the generation–recombination current J_{gr} and the current through the shunt:

$$J = J_{gr} + \frac{V}{R_{sh}}. \quad (10)$$

As seen in Fig. 6a, allowing for the action of the shunt using Eq. (10) leads to modification of the I–V characteristic shown by triangles. The exponential dependence of $J_{sc} \propto [\exp(qV/1.9kT) - 1]$ extends down to the lowest forward biases and the reverse currents coincide with the calculation results. When the reverse voltages are higher than 0.3 V another mechanism of charge transport (tunneling as previously mentioned) manifests itself.

5. Conclusions

We have investigated the electrical characteristics of CdS/$Cd_{0.92}Mg_{0.08}Te$ solar cells with bandgap of the absorber layer 1.60 eV. The coincidence between the theoretical data and the measured results show that the Sah–Noyce–Shockley generation–recombination theory developed earlier for interpretation of the electrical properties of thin-film CdS/CdTe solar cells are applicable for CdS/$Cd_{1-x}Mg_xTe$ structures as well. The theoretical predictions agree well with the experimental forward current in a wide range of bias voltages, where the current follows the dependence $I \propto [\exp(qV/nkT) - 1]$ with the ideality factor $n = 1.9$. The deviation of n from 2 is explained by the fact that according to the theory the dependence of the recombination current on the voltage is determined not only by the exponent $\exp(qV/2kT)$, but also by the pre-exponential factor $(E_g - 2\Delta\mu - qV)]^{-1/2}$. A comparison of the theoretical values with the experimental data allows us also to determine the main parameters of the material used and the diode structure such as: resistivity of the $Cd_{1-x}Mg_xTe$ absorber, concentration of holes in the valence band, Fermi level position, width and height of the barrier at the interface, lifetimes of charge carriers, and the ionization energy of the generation–recombination center. The need to reduce the resistivity of the $Cd_{1-x}Mg_xTe$ absorber layer causing too low barrier height in the heterostructure and unacceptable electrical losses in the solar cell have been discussed.

Acknowledgments

The study was supported by the State Foundation for Fundamental Investigations of Ukraine within the Project Φ40.7/014. The CdTe program at IER-UNAM was partially supported by the Projects SENER-CONACyT 117891, and CeMIE-Sol 207450/P25.

References

Bonnet, D., 2003. CdTe thin-film PV modules. In: Markvart, T., Castafier, L. (Eds.), Practical Handbook of Photovoltaics: Fundamentals and Applications. Elsevier Ltd, New York, pp. 333–366.

Compaan, A.D., Collins, R., Karpov, V.G., Giolando, D., 2008. Sputtered II–VI alloys and structures for tandem PV. Subcontract Report NREL/SR-520-43954 (2003–2007), pp. 1–50.

Coutts, T.J., Ward, J.S., Young, D.L., Gessert, T.A., Noufi, R., 2001. The search for and potential impact of improved transparent conducting oxides on thin-film solar cells. In: Technical Digest of the 12th International Photovoltaic Science and Engineering Conference, Jeju, Korea, p. 277–280.

Coutts, T.J., Ward, J.S., Young, D.L., Emery, K.A., Gessert, T.A., Noufi, R., 2003. Critical issues in the design of polycrystalline, thin-film tandem solar cells. Progr. Photovoltaics: Res. Appl. 11, 359–375.

Dhere, R., Ramanathan, K., Scharf, J., Moutinho, H., To, B., Duda, A., Noufi, R., 2006. Investigation of $Cd_{1-x}Mg_xTe$ alloys for tandem solar cell applications. In: Photovoltaic Energy Conversion, Conference Record of the IEEE 4th World Conference, vol. 1, 7–12 May, 2006. pp. 546–549.

Dhere, R., Ramanathan, K., Scharf, J., Young, D., To, B., Duda, A., Moutinho, H., Noufi, R., 2007. Fabrication and characterization of $Cd_{1-x}Mg_xTe$ thin films and their application in solar cells. Mater. Res. Soc. Symp. Proc. 1012, 37–42.

First solar sets another world record for CdTe solar PV efficiency, 2012. <http://investor.firstsolar.com/releasedetail.cfm?ReleaseID=639463>.

First solar sets world record for CdTe solar cell efficiency, 2014. <http://investor.firstsolar.com/releasedetail.cfm?ReleaseID=828273>.

Gessert, T.A., Metzger, W.K., Dippo, P., Asher, S.E., Dhere, R.G., Young, M.R., 2009. Dependence of carrier lifetime on Cu-contacting temperature and ZnTe:Cu thickness in CdS/CdTe thin film solar cells. Thin Solid Films 517, 2370–2376.

Gloeckler, M., Fahrenbruch, A.L., Sites, J.R., 2003. Numerical modeling of CIGS and CdTe solar cells: setting the baseline. In: Proceedings of 3rd World Conference on Photovoltaic Energy Conversion, vol. 1, Osaka, Japan, pp. 491–494.

Hartman, J.M., Cibert, J., Kany, F., Mariette, H., Charleux, M., Alleysson, P., Languer, R., Feuillet, G., 1996. CdTe/MgTe heterostructures: growth by atomic layer epitaxy and determination of MgTe parameters. J. Appl. Phys. 80, 6257–6265.

Hernández-Rodríguez, E., Rejón, V., Riech, I., Acosta, M., Peña, J.L., 2014. Morphological and chemical study of CdTe thin films annealed in $CHClF_2$–O_2 gas mixture. Sol. Energy 107, 305–313.

Ihn, Y.S., Kim, T.J., Ghong, T.H., Kim, Y.D., Aspnes, D.E., Kossut, J., 2004. Parametric modeling of the dielectric functions of $Cd_{1-x}Mg_xTe$ alloy films. Thin Solid Films 455–456, 222–227.

Kosyachenko, L.A., 2006. Problems of efficiency of photoelectric conversion in thin-film CdS/CdTe solar cells. Semiconductors 40 (6), 710–727.

Kosyachenko, Leonid, Toyama, Toshihiko, 2014. Current–voltage characteristics and quantum efficiency spectra of efficient thin-film CdS/CdTe solar cells. Sol. Energy Mater. Sol. Cells 120 (part B), 512–520.

Kosyachenko, L.A., Sklyarchuk, V.M., Sklyarchuk, O.V., Maslyanchuk, O.L., 2011. Band gap of CdTe and $Cd_{0.9}Zn_{0.1}Te$ crystals. Semiconductors 45, 1247–1250.

Kosyachenko, L.A., Mathew, X., Roshko, V. Ya., Grushko, E.V., 2013. Optical absorptivity and recombination losses: the limitations imposed by the thickness of absorber layer in CdS/CdTe solar cells. Sol. Energy Mater. Sol. Cells 114, 179–185.

Martinez, O.S., Reyes-Coronado, D., Mathew, X., 2009. $Cd_{1-x}Mg_xTe$ thin-films and top-cells for possible applications in tandem solar cells. Proc. SPIE 7409 Thin Film Sol. Technol. 20, 74090.

Martinez, S. Omar, Palomera, Roger C., Cruz, Jose S., Mathew, X., 2009. Co-evaporated $Cd_{1-x}Mg_xTe$ thin films for applications in tandem solar cells. Phys. Status Solidi C 6, S214–S218.

Mathew, X., Drayton, J., Parikh, V., Mathews, N.R., Liu, X., Compaan, A.D., 2009. Development of a semitransparent CdMgTe/CdS top-cell for applications in tandem solar cells. Semicond. Sci. Technol. 24, 015012.

McCandless, B.E., Sites, J.R., 2011. Cadmium telluride solar cells. In: Luque, A., Hegedus, S. (Eds.), Handbook of Photovoltaic Science and Engineering, second ed. John Wiley & Sons, Ltd., Hoboken, NJ, pp. 600–641.

Rejon, V., Riech, I., Pena, J.L., 2013. Study of CdS/CdTe solar cells activated with an oxygen–$CHClF_2$ gas mixture. Sol. Energy 95, 319–324.

Sah, C., Noyce, R., Shockley, W., 1957. Carrier generation and recombination in p-n junctions and p–n junction characteristics. Proc. IRE. 46, 1228.

Sites, J., Pan, J., 2007. Strategies to increase CdTe solar-cell voltage. Thin Solid Films 515, 6099–6102.

Sze, S.M., Ng, Kwok K., 2006. Physics of Semiconductor Devices, third ed. Wiley-Interscience, New Jersey.

Tatarenko, S., Baron, T., Arnoult, A., Cibert, J., Grun, M., Haury, A., Merle d Aubigne, Y., Wasiela, A., Saminadayar, K., 1997. Nitrogen doping of Te-based II–VI compounds. J. Cryst. Growth 175 (176), 682–687.

Toma, O., Ion, L., Girtan, M., Antohe, S., 2014. Optical, morphological and electrical studies of thermally vacuum evaporated CdTe thin films for photovoltaic applications. Sol. Energy 108, 51–60.

Waag, A., Heinke, H., Scholl, S., Becker, C.R., Landwehr, G., 1993. Growth of MgTe and $Cd_{1-x}Mg_xTe$ thin films by molecular beam epitaxy. J. Cryst. Growth 131, 607–611.